

Contents lists available at ScienceDirect

Fuel

journal homepage: www.elsevier.com/locate/fuel



Full Length Article

Accurate internal methane dry reforming kinetic models for solid oxide fuel cells

Saeed Moarrefi ^a, Mohan Jacob ^a, Shou-Han Zhou ^b, Stephen Skinner ^c, Lichao Jia ^{d,e}, Weiwei Cai ^f, Liyuan Fan ^{g,*}

- ^a College of Science and Engineering, James Cook University, Australia
- ^b Department of Mechanical Engineering, Cardiff University, UK
- ^c Department of Materials, Imperial College London, London, UK
- d Research Institute of Huazhong University of Science and Technology in Shenzhen, Shenzhen 518000, China
- ^e School of Materials Science and Engineering, State Key Lab of Materials Processing and Die & Mould Technology, Huazhong University of Science and Technology, Wuhan 430074, China
- f Faculty of Metallurgical and Energy Engineering, Kunming University of Science and Technology, Kunming 650093, China
- g School of Chemistry and Chemical Engineering, Queen's University Belfast, UK

ARTICLE INFO

Keywords: SOFC Dry Reforming Kinetics Power-Law Langmuir Hinshelwood–Hougen Watson, Electrochemical Reactions

ABSTRACT

Coupling with solid oxide fuel cells, methane dry reforming is a promising pathway for energy production from two greenhouse gases. However, the influence of carbon dioxide and electrochemical reactions on the internal dry reforming reaction within the fuel cells remains debatable, requiring accurate kinetic models to describe the internal reforming behaviors. In this study, we investigated the Power-Law and Langmuir Hinshelwood-Hougen Watson models in an electrolyte-supported solid oxide fuel cell with a NiO-GDC-YSZ anode to get accurate models for internal dry methane reforming. The current density used in this study ranges from 0 to 1000 A/m² at 973 K to 1173 K to estimate various kinetic parameters. The influence of the electrochemical reactions on the adsorption terms, the equilibrium of the reactions, the activation energy, the pre-exponential factor of the rate constant, and the adsorption equilibrium constant were studied. Furthermore, the adsorption enthalpy and entropy were investigated for the first time to understand the Gibbs free energy of CO₂ adsorption. The accuracy of kinetic models for estimating kinetic parameters was also evaluated. The dual-site models show better estimations than the other models and are then utilized to predict the reaction rate in the fuel cell. The derived kinetic parameters were consistent with values reported in the literature, confirming the reliability and general applicability of the developed models. For the first time, the adsorption enthalpy, entropy, and Gibbs free energy of CO₂ adsorption were quantified in a DRM-SOFC system, providing new thermodynamic insight into electrochemically influenced adsorption behavior. However, the dual-site LHHW models' accuracy was still insufficient, indicating a need for further research to develop a comprehensive kinetic model for internal dry reforming in fuel cells. This study provides essential parameters for future simulations and highlights the need for a more detailed examination of reforming kinetic models.

1. Introduction

In 2021, governments reasserted their commitment to attempt to limit global warming to $1.5~^{\circ}\text{C}$ as outlined in the Glasgow Climate Pact [1]. However, in 2023, the Earth experienced its highest recorded average surface temperature since 1880 [2]. Reliable actions are required to significantly and rapidly reduce the production and consumption of coal, oil, and gas [3]. CO_2 significantly impacts long-term

climate change, while methane immediately impacts climate change. Methane is a potent greenhouse gas that causes global warming, with human activities contributing to an estimated 60 % of current emissions [2]. Thus, both gases necessitate attention and comprehensive mitigation strategies to address their contributions to global warming effectively. Solid Oxide Fuel Cells (SOFCs) directly convert these two greenhouse gases (CO₂ and CH₄) into H₂, CO and electricity [4], which holds substantial promise for immediate contributions to limiting global warming. A primary advantage of SOFCs is the high combined heat and

E-mail address: l.fan@qub.ac.uk (L. Fan).

^{*} Corresponding author.

| Nomenclature | | k | |
|--|--|--|--|
| | | а | |
| Abbrevia | tions | b | |
| DRM SRM LHHW LH ER PL CFD RWGS SOFC NiO-YSZ | Dry Reforming of Methane Steam Reforming of Methane Langmuir-Hinshelwood-Hougen-Watson Langmuir-Hinshelwood Eley-Rideal Power Law Computational Fluid Dynamics Reverse Water Gas Shift Solid Oxide Fuel Cell Nickel-Yttria-Stabilized-Zirconia C Nickel-Gadolinium-Doped-Ceria Rate Determining Step Mass Flow Controller Gas Chromatograph Triple Phase Boundary Open Circuit Voltage | b R θ $Subscripts$ X_{CH_4} $F_{CH_4}^{inlet}$ $F_{CH_4}^{outlet}$ W_{cat} r_{CH_4} k_0 p_j K_j A_j ΔH_j^0 ΔS_j^0 | |
| RMSE R ² | Root mean square error coefficient of determination | K_{DRM}^{eq} K_{RWGS}^{eq} | |
| Latin syr | nbols | df | |
| P D | | E_a | |
| R T | | | |

power efficiency, enabling simultaneous electricity and heat production [5,6], while emitting substantially lower carbon than conventional energy systems by refeeding the anode off-gas to the inlet [7,8]. However, the rapid internal endothermic reforming process within SOFCs can result in severe local thermal stress, leading to long-term performance degradation[9]. Besides that, high catalytic activity at the anode's surface may increase the carbon deposition rate, further impose cell stress and potentially cause cracks over extended periods of operation[5,7]. Since the performance of a SOFC is significantly influenced by the type of anode and the fuel being employed, an anode with a balance of electronic conductivity, redox stability, and resistance to sulfur and cocking are needed [10]. Understanding the mechanism and kinetics of this process is the critical strategy to guide the improvement of anode materials, ultimately leading to fabricating more cost-effective and robust SOFCs.

Studies on the kinetics and mechanism of dry reforming of methane (DRM)[4,11–13] have been conducted; however, they are still limited. More comprehensive studies are needed to better understand the various mechanisms involved, particularly with different catalysts and operating conditions[11]. Furthermore, there is still considerable debate about applying those models for internal DRM inside SOFCs (DRM-SOFC). Consequently, various kinetic models, such as the Power-Law (PL), Eley-Rideal (ER), Langmuir Hinshelwood (LH), and Langmuir Hinshelwood-Hougen Watson (LHHW), have been proposed in the literature[11,14-16]. The PL model has been widely utilized for determining the kinetics of DRM[17] because of its straightforward application in determining reaction orders. However, the PL models did not consider the multiple steps involved in the reaction mechanism on the catalyst surface [18]. The ER model proposes a mechanism wherein the reaction occurs between substances adsorbed on the catalyst surface and those in the gas phase, ultimately producing the desired products [19]. The LH model has garnered significant attention due to its alignment with experimental findings[20], such as recent studies by Li et al.[21], Nakajima et al. [22], and Wittich et al. [23], where both reactants initially adsorb onto the catalyst surface before undergoing a reaction between the adsorbed species to generate the desired products [11]. This approach has led to the development of different kinetics equations within the LH mechanism, including the single-site and dual-site models [19]. The LH model is more straightforward, focusing only on the bimolecular reaction steps[15]. The LHHW model extends the LH model by considering the surface concentrations of the species participating in the reaction, and it relates the surface species to the observed species' partial pressures in the gas phase.

Fan et al. [24] conducted experiments on Ni-GDC anodes, exploring various gas compositions, operating temperatures, and current densities to gather kinetic data for Computational Fluid Dynamics (CFD) modeling of methane steam reforming (SRM) inside SOFCs (SRM-SOFC). They employed a power-law kinetic model due to its simplicity and compatibility with CFD models. Their findings indicated a slight increase in SRM reaction rate with current density application and a positive correlation with methane concentration enhancement. While the obtained kinetic parameters are suitable for integration into CFD simulations, their study lacked consideration of alternative kinetic models for a more precise evaluation of kinetics over SRM-SOFC. Thallam Thattai et al.[25] emphasized the necessity of developing readily applicable kinetic models, building upon intrinsic models previously reported. Their study compared PL and LH models in SRM-SOFC to analyze the limitations of previously proposed rate expressions by Fan et al.[24] on Ni-GDC anodes. Both proposed kinetic models predict distinct SRM reaction rates and species partial pressure distributions along the normalized reactor length, highlighting the need for additional experimental and modeling verifications. To cover the gaps mentioned earlier in the research, Fan et al. [26] conducted experiments on a Ni-YSZ anode to investigate the impact of operating parameters on SRM kinetics for both PL and LH kinetic models. The evaluation of the models revealed that the additional parameters in the LH model led to a lower mean absolute percentage error and a higher coefficient of determination (R^2) . This finding supports the idea that the LH kinetic model describes the reaction rate more accurately than the PL model in SRM-SOFC. Zhou et al. [27] also mentioned that the impact of steam and current density on SRM-SOFC has been a subject of ongoing debate. Developing appropriate kinetic models to describe SRM behavior under

various temperatures and current densities accurately is crucial. The LH model proposed in their study demonstrated better accuracy in describing reforming rates and kinetics at a current density of 600 A/m² than open-circuit and 1000 A/m² conditions. A recent article by Wojcik et al. [28] has emphasized that more complex equations for methane reforming do not necessarily result in more accurate outcomes. Furthermore, they concluded that such mathematical models for the SRM are often applicable within a very narrow temperature range, which should be the primary consideration when selecting an equation for a specific fuel cell. However, SRM-SOFCs have garnered significant attention in the literature, and limited information regarding the influence of electrochemical reactions on the kinetics parameters of DRM-SOFC is available. The authors of this study recently explored the effects of temperature, gas composition, and current density on the kinetics parameters of DRM within an electrolyte-supported NiO-GDC-YSZ button cell, employing both PL and simplified LH kinetic models[4]. We found that the CH₄ partial pressure has a more pronounced effect on DRM reaction rate than CO₂, especially at higher temperatures where reaction rates are enhanced by facilitating chemical bond breakdown. Furthermore, increased current density leads to higher CO₂ adsorption equilibrium constants and enhanced methane conversion. The changes in reaction orders, activation energy, pre-exponential factors, and adsorption kinetic parameters under the influence of electrochemical reactions for DRM-SOFC were studied. Numerous studies have been conducted on the kinetics and mechanism of the SRM-SOFC. However, there is still no agreement on a common kinetic model for DRM-SOFC systems, indicating that the reaction kinetics strongly depend on the process and anode material used. To facilitate the widespread application of the DRM-SOFC technology in industry, understanding the mechanism of this process is essential [24,28-30]. Furthermore, internal DRM mechanisms in SOFC have not been extensively studied. This study investigates different kinetic models with various parameters, including reaction orders, adsorption equilibrium constants, and activation energies, that best describe the DRM reaction over the NiO-GDC-YSZ anode in an SOFC. Also, previous kinetic investigations of DRM and SRM in SOFCs have primarily focused on reaction orders, rate constants, and activation energies, while the thermodynamic characteristics of gas adsorption on the anode surface have rarely been examined. In contrast, this study provides the first systematic estimation of the adsorption enthalpy, entropy, and Gibbs free energy of CO2 adsorption in a DRM-SOFC systems. These parameters reveal how temperature and electrochemical reactions influence the spontaneity and strength of CO₂ adsorption on the Ni-GDC-YSZ anode, thereby linking surface thermodynamics with kinetic behavior. This combined thermodynamic and kinetic approach offers a new perspective for understanding electrochemically driven adsorption phenomena inside fuel cells and distinguishes this work from earlier reforming studies.

2. Methodology

2.1. Experiment

The experimental data utilized in this study were acquired from an electrolyte-supported button cell with NiO-GDC-YSZ anode, as detailed in our prior research[4]. The developed model describes intrinsic DRM kinetics on anode side, with rate expressions derived under conditions minimising heat and mass transfer effects. A button cell with a geometric area of $0.95~\rm cm^2$, featuring a 1 cm diameter and 50 μ m thickness, was employed using a catalyst mass of 14.3 mg in accordance with International Confederation for Thermal Analysis and Calorimetry (ICTAC) recommendations (<1 g) to avoid transport limitations[31,32]. Before experimentation, the anode was reduced with hydrogen following heating to 1173 K in a nitrogen atmosphere. Subsequently, the anode was gradually exposed to a reducing atmosphere for 4 h using hydrogen while maintaining a total flow rate of 8 ml/min. The cathode was exposed to ambient air throughout the whole experiment. Then, the

experiments were conducted at open circuit and current densities of 500 $\rm A/m^2$ and 1000 $\rm A/m^2$, employing varying gas inlet flow rates containing CH₄ and CO₂. Gas flow to the fuel cell was regulated by mass flow controllers (MFC). The current density range of utilized in this study corresponds to total currents of 0.095 A for the present geometry, or 2.5 A and 10 A for cell areas of 25 cm² and 100 cm², respectively. Moisture contained in the anode outlet was removed by a condenser and silica gel desiccant bed, followed by gas composition analysis using a Shimadzu Nexis Gas Chromatograph (GC-2030). Two additional temperature sets were incorporated into the previous study to enhance the accuracy of the kinetic models [4]. As a result, the data in this study related to the five selected temperatures from 973 K to 1173 K. Five different biogas compositions were considered in this study, as outlined in Table 1, and methane conversions under various working conditions are available in Table 2.

Additional information supporting this study is provided in the Supplementary Material (Appendix A). This includes a detailed description of the experimental setup and test station, inlet gas compositions and methane conversion data under various operating conditions, and the complete MATLAB® scripts used for kinetic parameter estimation. The supplementary file also outlines the thermodynamic validation criteria and calculation guidelines applied to evaluate adsorption equilibrium constants and rate expressions.

2.2. Kinetic models

In catalytic studies, fixed-bed reactors are widely used to evaluate intrinsic activity under controlled conditions, as they allow precise temperature control and isolation of the chemical reaction from electrochemical effects. However, they do not replicate the coupled catalytic-electrochemical environment presents inside a SOFC. In contrast, the narrow porous paths in the SOFC anode and low back-mixing allow the system to be approximated as an ideal plug-flow reactor (PFR), enabling the direct study of dry reforming kinetics under simultaneous electrochemical operation. Although a continuous stirred-tank reactor (CSTR) model would assume complete mixing, the unidirectional gas transport through the porous anode makes such behavior unlikely in this configuration. In this work, the cumulative catalyst mass W_{cat} is treated as the equivalent reactor length, and a steady-state mole balance is applied across small catalyst elements. The small catalyst mass (14.3 mg) and high inlet gas flow rates minimize transport effects in accordance with ICTAC recommendations, while the 0.95 cm² button cell geometry ensures a short diffusion path and directional gas transport. The inlet gas flow rates were intentionally set much higher than the electrochemical consumption rate, ensuring a non-equilibrium status in the SOFC. Also, in small-scale SOFCs, not all inlet gas reaches triplephase boundary sites due to flow distribution, porosity, and limited penetration, so some fuel bypasses unreacted[33]. Short diffusion paths also promote rapid gas-phase homogenization, reducing concentration gradients[34,35]. While this benefits intrinsic kinetic measurements, larger commercial cells often exhibit less uniform gas/electrode contact and more pronounced gradients, affecting apparent reaction rates[35]. Full details of the PFR assumption, partial pressure calculations, and side reaction treatments are provided in the Supplementary Material. This approach allows realistic assessment of reaction behavior under actual

Table 1
Inlet biogas compositions[4].

| Case No. | Compositi CH ₄ | on (%) CO ₂ | N_2 | Total flow rate nml/min | $\mathrm{CH_4} / \mathrm{CO_2}$ R |
|---------------------------|------------------------------|------------------------------|------------------------------|-------------------------|-------------------------------------|
| i ii iii iv v | 30 30 40 50 | 60 40 40 40 33.3 | 10 30 20 10 16.7 | 8 8 8 8 | 0.5 0.75 1 1.25 |

Table 2Methane conversions under various operational conditions[4].

| | | Overall N | Overall Methane Conversion (%) | | | | |
|--------------------|---|-----------|--------------------------------|-------|-------|-------|--|
| Temperature [K] | Current Density [A/m ²] | i | Ii | Iii | Iv | v | |
| 973 | 0 | 0.174 | 0.161 | 0.139 | 0.128 | 0.127 | |
| | 500 | 0.189 | 0.177 | 0.150 | 0.142 | 0.136 | |
| | 1000 | 0.213 | 0.201 | 0.174 | 0.158 | 0.154 | |
| 1023 | 0 | 0.209 | 0.193 | 0.171 | 0.161 | 0.161 | |
| | 500 | 0.219 | 0.209 | 0.182 | 0.179 | 0.171 | |
| | 1000 | 0.245 | 0.234 | 0.206 | 0.190 | 0.188 | |
| 1073 | 0 | 21.90 | 20.60 | 18.40 | 17.30 | 17.20 | |
| | 500 | 23.40 | 22.20 | 19.50 | 18.70 | 18.10 | |
| | 1000 | 25.80 | 24.60 | 21.90 | 20.30 | 19.90 | |
| 1123 | 0 | 24.10 | 22.80 | 20.10 | 19.00 | 18.90 | |
| | 500 | 25.20 | 24.00 | 22.20 | 20.40 | 19.90 | |
| | 1000 | 27.40 | 26.20 | 23.90 | 22.00 | 21.60 | |
| 1173 | 0 | 22.10 | 21.90 | 21.80 | 21.60 | 21.40 | |
| | 500 | 23.00 | 22.80 | 21.90 | 21.70 | 21.60 | |
| | 1000 | 26.20 | 25.10 | 24.00 | 22.80 | 22.50 | |

cell operating conditions.

Syngas, which contain H_2 and CO, could be generated during the catalytic oxidation reaction of biogas (CO_2 and CH_4) in the DRM, in reaction (1)[8].

$$CH_4 + CO_2 \rightleftarrows 2CO + 2H_2 \tag{1}$$

The hydrogen produced in DRM reacts with oxygen ions (O⁻²) from the electrolyte to produce water molecules (H2O), release electrons and generate electricity[36,37]. Proper derivation, evaluation, and reporting of rate data for DRM-SOFC are essential based on reaction models, which depend on both anode material and process conditions. Due to the conformity of most of the mechanical steps in Langmuir models with experimental data of DRM[15,28], LHHW theory can be conducted for the kinetic modeling of DRM-SOFC in this study. According to this theory, reactive molecules are adsorbed onto the active sites of the catalyst on the anode surface, where they undergo surface reactions to form products. Subsequently, when these weak bonds are broken, the reaction products are released from the active sites. In this model, either the substance adsorption step or the surface reaction of the adsorbed species is accepted as the rate-determining step (RDS). For the catalytic DRM, the reaction occurs according to the following five stages: (1) CH₄ adsorption, (2) CO₂ adsorption, (3) surface reaction of adsorbed species, (4) desorption of CO, and (5) desorption of H₂[11]. In this mechanism, we assume that the adsorption of CH₄ and CO₂ at the catalyst surface (step 3) is considered the RDS[15] which assumes that it is the slowest step, while the others are in thermodynamic equilibrium while determining the overall kinetics.

Furthermore, the RDS often involves the adsorption or desorption of reactants or intermediates on the anode surface, which can vary depending on the nature of the catalyst[17]. The forward water–gas shift (WGS) reaction was not considered because the system operates under dry reforming conditions with no steam addition, at temperatures above 973 K and in a CO₂-rich environment. Thermodynamically, these conditions strongly favor the Reverse Water-Gas Shift (RWGS) reaction, making the forward WGS rate negligible. The RWGS pathway, which consumes H_2 and produces CO and H_2 O, was therefore included in the model and assumed to be at equilibrium, with the formulation and equilibrium constant correlations provided in the Supplementary Material. Additionally, we assume that the RWGS reaction is much faster than the DRM reaction and is at equilibrium. By considering the assumptions mentioned above, the general rate expression for the LHHW model can be described by Eq. (1)[25,27]:

$$r = \frac{(\text{Kinetic Factor})}{(\text{Adsorption Term})}(\text{Driving Force})$$
 (2)

In the current study, we aim to investigate the influence of individual parameters in rate expression, such as kinetic factors, adsorption terms, and driving force, on the estimation accuracy of kinetic parameters for DRM-SOFC. The driving force (*df*) is the coefficient that accounts for the inverse reaction and indicates the direction of the equilibrium reaction, is provided by Eq. (2) [4,11,15]:

$$df = 1 - \frac{p_{\rm CO}^2 p_{\rm H_2}^2}{K_{\rm DRM}^{\rm eq} p_{\rm CH_4} p_{\rm CO_2}}$$
 (3)

Where $p_{\rm CO}$, $p_{\rm H_2}$, $p_{\rm CH_4}$ and $p_{\rm CO_2}$ are the partial pressures (bar) for CO, H₂, CH₄, and CO₂, respectively. The term $K_{\rm DRM}^{\rm eq}$ is the DRM equilibrium constant which is determined by Eq. (3)[16]:

$$K_{\rm DRM}^{\rm eq} = 6.78 \cdot 10^{14} \cdot \exp(\frac{-259660}{RT})$$
 (4)

Where R is the Universal gas constant, and T is Temperature in K. Since this model assumes the presence of different active sites, including metallic single-site or dual-sites, researchers have proposed several alternative and occasionally conflicting kinetic models for DRM. Since intrinsic kinetic parameters are independent of electrode geometric area, the rate constants and adsorption coefficients determined here can be applied directly to larger commercial-scale cells, provided that appropriate transport and thermal management models are included for stack-level simulations. It is crucial to thoroughly investigate these models for their accuracy and applicability in electrochemical devices such as SOFCs. The kinetic models derived from the literature based on the abovementioned reaction pathways are summarized in Table 3.

For clarity, in this study, LHHW-1 and LHHW-2 refer to single-site models (without and with inverse reaction terms, respectively), whereas LHHW-3 and LHHW-4 correspond to dual-site models (without and with inverse reaction terms).

The actual DRM reaction rate in a flow system in the gas phase from experiment data is represented by the actual reaction rate in Table 3. $F_{\rm CH_4}^{\rm inlet}$ represents the methane flow rate (in mol/s) in the inlet gas mixture, $X_{\rm CH_4}$ denotes the methane conversion, and $W_{\rm cat}$ stands for the mass of catalyst loading on the anode (in grams). In the DRM rate expression, for PL and LHHW models, 'a' represents the reaction order for methane, while 'b' denotes the reaction order for carbon dioxide. These coefficients indicate how gas concentrations influence the reaction rate. In single site-LHHW models, θ represents the surface coverage. When the steady-state surface coverage of a reactant molecule is nearly complete and represents high surface coverage, this term equals 1 ($\theta=1$). This situation is typical for strongly adsorbing species or under high-pressure conditions.

In contrast, the value of $\theta=0.5$ indicates that the reaction occurs in the medium coverage region, which is typical for weakly adsorbing species or under low-pressure conditions. Tri Nguyen et al. [11] utilized

Table 3Selected PL and LHHW Models for NiO-GDC-YSZ anode for SOFC.

| Model | Kinetic Model | Rate Expression |
|------------|-----------------------------------|--|
| AC | Actual reaction rate | $r_{\text{Actual}} = \frac{F_{\text{CH}_4}^{\text{inlet}}}{W_{\text{cat}}} X_{\text{CH}_4}$ |
| PL | Power Law | $r_{\mathrm{PL}} = k (p_{\mathrm{CH_4}})^a (p_{\mathrm{CO_2}})^b$ |
| LHHW- 1 | Single site | $r_{	ext{LHHW}-1} = rac{k ig(p_{	ext{CH}_4}ig)^a ig(p_{	ext{CO}_2}ig)^b}{[1 + K_{	ext{CH}_4}p_{	ext{CH}_4}^a + K_{	ext{CO}_2}p_{	ext{CO}_2}^b]^{2	heta}}$ |
| LHHW- 2 | Single site with inverse reaction | $r_{\text{LHHW}-2} = \frac{k(p_{\text{CH}_4})^a (p_{\text{CO}_2})^b}{[1 + K_{\text{CH}_4} p_{\text{CH}_4}^a + K_{\text{CO}_2} p_{\text{CO}_2}^b]^{2\theta}} (df)$ |
| LHHW- 3 | Dual site | $r_{\text{LHHW}-3} = \frac{k(p_{\text{CH}_4})^a(p_{\text{CO}_2})^b}{\left[1 + (K_{\text{CH}_4}p_{\text{CH}_4})^a\right]\left[1 + (K_{\text{CO}_2}p_{\text{CO}_2})^b\right]}$ |
| LHHW- | Dual site with inverse | $r_{\text{LHHW}-4} =$ |
| 4 | reaction | $\frac{k(p_{\text{CH}_4})^a(p_{\text{CO}_2})^b}{\left[1+(K_{\text{CH}_4}p_{\text{CH}_4})^a\right]\left[1+(K_{\text{CO}_2}p_{\text{CO}_2})^b\right]}(df)$ |

the least-squares optimization method to compute DRM reaction orders and kinetic constant values using the single-site LHHW model with varying θ values from 0 to 1. The root-mean-square error (RMSE) and R^2 values of the calculated reaction rates indicated the best fit with the experimental data when assuming the reaction occurs in the medium coverage region ($\theta=0.5$). Furthermore, the gas pressure inside the fuel cell remains low, approximately at atmospheric pressure conditions. Therefore, the medium surface coverage assumption was adopted in this study.

In the LHHW models, the adsorption terms are described by the adsorption coefficients of carbon dioxide (K_{CO_2}) and methane (K_{CH_4}) . For this study, the CH₄ adsorption coefficient is assumed to depend solely on temperature. The change of adsorption enthalpy $\Delta H_{CH_4}^0 = -38.28 \, (kJ/mol)$ and pre-exponential factor of methane adsorption $A_{CH_4} = 0.000665$ were used in this study[4,26,27]. Given that the DRM reaction primarily takes place on the outer surface of the anode, with CH₄ diffusing into the anode from the bulk flow, the adsorption parameters for CH₄ are considered unaffected by the changing current density in this study[27]. The optimized parameters were determined, including the reaction order of carbon dioxide (b), the adsorption coefficient, and the reaction rate constant (k). Most DRM modelling studies typically assume a first-order reaction rate for methane to simplify calculations. In this study, the coefficient 'a' in the rate expressions for LHHW models equals 1[38]. The adsorption coefficient was calculated by using the Van't Hoff equation (Eq.(4)) as follows[25]:

$$K_{\text{CO}_2} = A_{\text{CO}_2} \cdot \exp\left(-\frac{\Delta H_{\text{ad}}^0}{RT}\right) \tag{5}$$

Where $A_{\rm CO_2}$ represents the pre-exponential factor for the ${\rm CO_2}$ adsorption constant, $\Delta H_{\rm ad}^0$ denotes the enthalpy change for the adsorption of ${\rm CO_2}$. The adsorption constant must be thermodynamically consistent, which requires meeting three thermodynamic rules and two guidelines available in the Supplementary Materials[27]. The change in entropy for ${\rm CO_2}$ adsorption,

 ΔS_{ad}^0 , is subsequently calculated utilizing the adsorption constants in Eq.(5)[26]:

$$\Delta S_{\rm ad}^0 = \log(A_{\rm CO_2}) \times R \tag{6}$$

The change in Gibbs free energy of adsorption, $\Delta G_{\rm ad}^0$, indicates the spontaneity of a chemical adsorption reaction, making it a crucial criterion in determining spontaneity. Both adsorption enthalpy and entropy factors are necessary for calculating the Gibbs free energy of adsorption using Eq.(6)[19,26]. Adsorption reactions proceed spontaneously at a given temperature or current density when ΔG^0 is negative and a non-spontaneous process if it is positive[19].

$$\Delta G_{\rm ad}^0 = \Delta H_{\rm ad}^0 - T \Delta S_{\rm ad}^0 \tag{7}$$

For each model, the reaction rate constant was calculated by using Eq. (7) as follows[27]:

$$k = \frac{F_{\text{CH}_4}^{\text{inlet}}}{W_{\text{cat}}} \int_0^{X_{\text{CH}_4}^{\text{outlet}}} \frac{1}{r_{\text{CH}_4}^{\text{PL or LH}}} dX_{\text{CH}_4}$$
(8)

The Arrhenius equation for the rate constant of DRM is represented by Eq.(8)[39]:

$$k = k_0 \exp(\frac{-E_a^{\text{DRM}}}{RT}) \tag{9}$$

$$ln(k) = ln(k_0) - \frac{E_{\rm a}^{\rm DRM}}{R} \frac{1}{T}$$
(10)

In the equation, $E_{\rm a}^{\rm DRM}$ represents the activation energy, and k_0 is the preexponential factor for the DRM-SOFC reaction, respectively. The values of $E_{\rm a}$ and k_0 were determined through an iterative approach in MATLAB®, using the calculation algorithm and developed code provided in the Supplementary Materials. For the LHHW and PL models, the reaction orders were constrained to lie within the range of -2 to +2 to obtain results that fall within a reasonable range compared to values reported in the literature [40]. As observed from the comparison between Eq. (8) and rate expression in Table 3, respectively, k for the PL model depends on optimizing a and b, while for the LHHW model, k relies on optimizing a, b, $K_{\rm CO_2}$ and $K_{\rm CH_4}$. In this study, the variation of CH₄ and CO₂ reaction order with current density was obtained directly from the kinetic parameter fitting. No explicit electrochemically activated reaction pathway was included in the model; instead, the effect of current density is reflected as a change in the apparent kinetic constant, capturing the influence of electrochemical operation on the observed kinetics.

3. Results and discussion

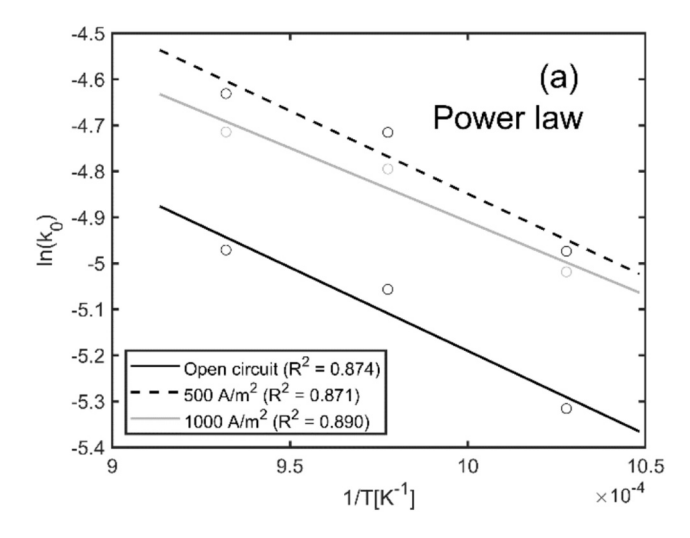
Complex models capture intricate details in chemical reaction kinetic studies, while simple models often yield meaningful insights compared to complex models. Simplicity allows us to focus on essential features, aiding our understanding of reaction pathways and rates [41]. This study evaluates how well kinetic models align with experimental data for DRM-SOFCs. The PL model ignores surface chemistry, while the all LHHW models (LHHW-1 to LHHW-4) includes reactant adsorption. Both models and their derivatives were used to examine the impact of electrochemical reactions on $\rm CO_2$ adsorption on a NiO-GDC-YSZ anode. Due to the lack of data on different kinetic models for DRM-SOFCs, direct comparisons with other studies are limited, indicating a critical research gap. Comparing these models would improve our understanding of kinetic factors and reaction rates. Arrhenius plots are essential for validating models, predicting reaction rates, and optimizing fuel cell operations.

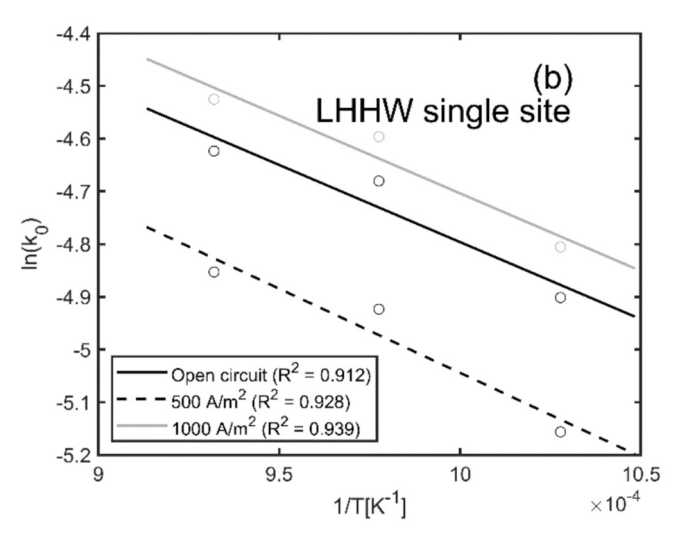
Fig. 1(a) to 1(c) show the Arrhenius plots for each proposed model, illustrating the relationship between the rate constant, temperature, current density, and activation energy, with corresponding R^2 values indicating the precision and reliability of the estimates. The derived kinetic parameters, including the reaction order of CO_2 and various kinetic factors, are presented in Table 4. The results, discussed in the following sections, highlight that the dual-site models exhibit the highest R^2 values, and generally provide a better fit than the PL model, with LHHW-3 and LHHW-4 models performing the best at 1000 A/m^2 .

3.1. Carbon dioxide reaction order

The CO_2 reaction order (b) in the rate equation describes the mathematical relationship between the rate of the reforming reaction and the CO_2 concentration, and it indicates to what extent the concentration of CO_2 affects the reaction rate.

Fig. 2 shows the current density dependence of the CO₂ reaction order predicted by each model. Results indicate this parameter ranges from 0.29 to 0.32 across temperatures from 973 K to 1173 K and current densities from open circuit to 1000 A/m2. The PL model shows a significant increase in CO2 reaction order with current density, peaking near 500 A/m². In contrast, the single-site (LHHW-1, LHHW-2) and dual-site (LHHW-3, LHHW-4) models show similar reaction order values display similar reaction order values up to 500 A/m², with differing trends at higher currents. Single-site models show a decrease followed by a slight increase in CO₂ reaction order, while dual-site models exhibit a decreasing trend across all current densities. The lack of CO2 reaction order data for DRM-SOFC prevents direct comparisons, but similar nonuniform trends have been observed in SRM-SOFC studies by Thattai et al.[25], Fan et al.[26] and Zhou et al.[27] in SRM-SOFC. Analysis of our recent study[4] revealed a decrease in CO2 reaction order with increasing current at temperatures from 1073 K to 1173 K. Dual-site models may provide better estimations across a wider temperature range. Differences between single-site and dual-site models are reflected





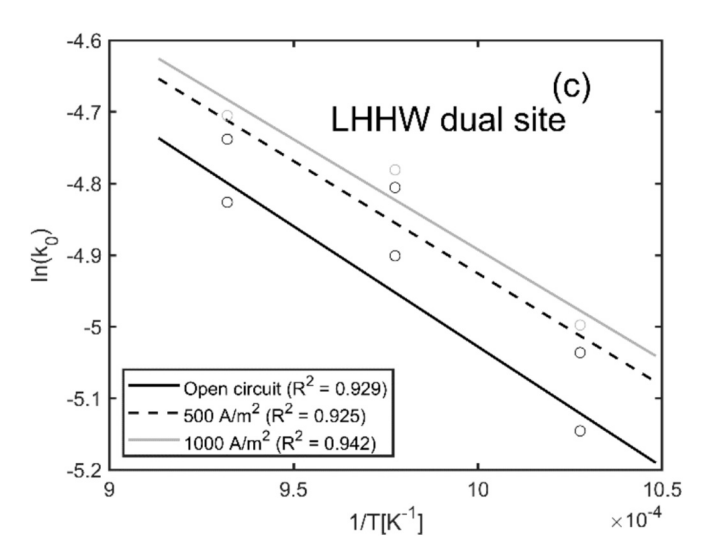


Fig. 1. Arrhenius plots used to determine and fit reaction parameters, including the coefficient of determination (R^2) , for (a) the Power-Law model, (b) LHHW single site models (LHHW-1, LHHW-2), and (c) LHHW dual site models (LHHW-3, LHHW-4).

in their adsorption terms, but current density minimally impacts ${\rm CO_2}$ reaction order. The equilibrium or reverse reaction has negligible effects on model estimations.

To assess the validity of the derived kinetic parameters, the results obtained in this study were compared with those reported in previous DRM and SRM kinetic studies over Ni-based catalysts. The activation energies for DRM-SOFC (17.9—24.8 kJ mol $^{-1}$) fall within the reported ranges for Ni-ceria and Ni-YSZ systems [11–13,15,17]. Similarly, the $\rm CO_2$ reaction orders (0.29—0.32) observed here correspond well with those found in SRM-SOFC studies by Thattai et al. [25], Fan et al. [26], and Zhou et al. [27], which ranged between 0.25 and 0.40. The estimated adsorption enthalpy and entropy are consistent with values reported for $\rm CO_2$ adsorption on Ni-based catalysts [15,19,35]. This agreement demonstrates that the kinetic parameters derived in the present work are physically realistic and comparable to those in the literature.

3.2. Activation energy (E_a)

Fig. 3 illustrates the influence of current density on the activation energy, showing a decrease from OCV to 1000 A/m² in all proposed models. The LHHW-3 and LHHW-4 models yield lower activation energy values compared to the PL model with the same current density, reflecting its consideration of surface reaction mechanisms[17]. Differences in the "adsorption term" between single-site and dual-site LHHW models result in varying activation energies at higher current densities. The reverse reaction has negligible effects on the obtained activation energies, aligning with trends observed in previous studies on DRM[4] and the SRM [24-26]. The decrease in activation energy in an SOFC is due to the current, which drives non-spontaneous reactions by lowering the activation energy. Electrochemical reactions serve as electrocatalysts, providing alternative pathways for hydrogen production with lower energy requirements [42]. This study does not expand upon the potential reasons for this research and does not delve into the reasons for the decreasing activation energy with increasing current density. Still, more details can be found in our recent study[4].

3.3. Pre-exponential factor of the reaction rate constant (k_0)

In chemical kinetic studies, the pre-exponential factor is an essential constant in the Arrhenius equation (Eq. (8)[43]. This factor signifies the frequency of collisions between CO_2 and CH_4 molecules [44]. It varies with temperature due to its connection to molecular collisions, which fluctuate accordingly [45]. Our results indicate that, in addition to temperature, k_0 may exhibit current density dependence, and its units may vary based on the CO_2 and CH_4 reaction orders.

Fig. 4 illustrates the impact of current density on the k_0 , demonstrating a decrease from OCV to 1000 A/m² across all four LHHW models (LHHW-1 to LHHW-4), with no significant difference observed. The PL model estimates a higher reaction order for CO_2 at 500 A/m^2 , causing k_0 to peak at this point and decrease with a higher current density. The numerator and denominator in the LHHW model(s) rate expressions have a negligible effect on the estimation accuracy of k_0 for DRM-SOFC systems. Both PL and all four LHHW models (LHHW-1 to LHHW-4) exhibit non-uniform trends across the investigated current densities, with similar values at higher current densities. Due to the absence of data on k_0 dependency on current density, direct comparisons with other literature are limited. Future work is needed to gather more experimental data on k_0 dependency for DRM-SOFCs.

3.4. Pre-exponential factor of the adsorption constant (A_{CO_2})

The pre-exponential factor, often denoted as $A_{\rm ad}$ in the context of the van 't Hoff in Eq.(4), relates to the temperature dependence of the adsorption equilibrium constant. This constant accounts for the frequency of adsorption—desorption events at a standard concentration and

Table 4
Derived kinetic parameters for proposed models across different current densities from 973 K to 1173 K. LHHW-1 and LHHW-2 (single-site) and LHHW-3 and LHHW-4 (dual-site) model predictions.

| Kinetic Parameters | Current Density [A/m ²] | PL | LHHW-1 | LHHW-2 | LHHW-3 | LHHW-4 |
|---------------------------------------|-------------------------------------|---------|---------|---------|----------|----------|
| Reaction order (b) | Open-Circuit | 0.29 | 0.31 | 0.31 | 0.31 | 0.31 |
| | 500 | 0.38 | 0.31 | 0.31 | 0.31 | 0.31 |
| | 1000 | 0.31 | 0.32 | 0.32 | 0.30 | 0.30 |
| E _a (kJ/mol) | Open-Circuit | 24.8 | 23 | 23.1 | 22.9 | 22.9 |
| | 500 | 23 | 19.7 | 19.7 | 19.6 | 19.6 |
| | 1000 | 19.7 | 17.9 | 17.9 | 18.9 | 18.9 |
| K_0 (mol/s g bar $^{(a+b)}$) | Open-Circuit | 1.1E-01 | 1.0E-01 | 1.0E-01 | 1.0E-01 | 1.0E-01 |
| | 500 | 1.3E-01 | 7.8E-02 | 7.8E-02 | 7.7E-02 | 7.7E-02 |
| | 1000 | 8.0E-02 | 7.2E-02 | 7.2E-02 | 7.3E-02 | 7.3E-02 |
| $\mathbf{A}_{\mathbf{CO}_2}$ | Open-Circuit | _ | 3.1E-06 | 3.1E-06 | 4.0E-06 | 4.0E-06 |
| _ | 500 | _ | 4.7E-6 | 4.7E-6 | 5.2E-06 | 5.2E-06 |
| | 1000 | _ | 2.6E-06 | 2.6E-06 | 1.0E-10 | 1.0E-10 |
| K_{CO_2} | Open-Circuit | _ | 8.6E-03 | 8.5E-03 | 1.1E-03 | 1.1E-03 |
| | 500 | _ | 1.3E-10 | 1.3E-10 | 1.4E-03 | 1.4E-03 |
| | 1000 | _ | 7.2E-04 | 7.2E-05 | 1.0E-10 | 1.0E-10 |
| $\Delta H_{CO_0}^0$ (kJ/mol) | Open-Circuit | _ | -50.2 | -50.2 | -50.2 | -50.2 |
| CO ₂ () | 500 | _ | -50.2 | -50.2 | -50.1 | -50.1 |
| | 1000 | _ | -50.1 | -50.1 | -4.5E-03 | -2.3E-03 |
| $\Delta S_{\text{CO}_0}^0$ (J/mol. K) | Open-Circuit | _ | -10.5 | -10.5 | -10.3 | -10.3 |
| | 500 | _ | -10.2 | -10.2 | -10.1 | -10.1 |
| | 1000 | _ | -10.7 | -10.7 | -19.1 | -19.1 |
| \mathbb{R}^2 | Open-Circuit | 0.874 | 0.930 | 0.930 | 0.929 | 0.929 |
| | 500 | 0.871 | 0.925 | 0.925 | 0.925 | 0.925 |
| | 1000 | 0.890 | 0.938 | 0.938 | 0.942 | 0.942 |

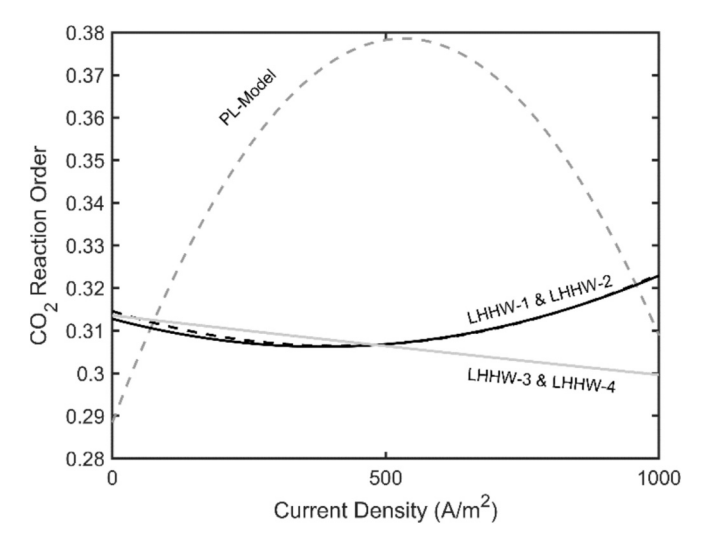


Fig. 2. The trend analysis of the current density effects on CO_2 reaction orders in each proposed model. The grey dashed line corresponds to the PL model, the black solid line represents the single-site models (LHHW-1, LHHW-2), and the grey solid line corresponds to the dual-site models (LHHW-3, LHHW-4).

reflects how often adsorbed CO_2 species transition between the surface and the gas phase [19]. Researchers use the van 't Hoff equation and the pre-exponential factor to understand how adsorption behavior changes with temperature [46]. In this study, A_{CO_2} is also influenced by the current density in the fuel cell.

Fig. 5 illustrates the current density-dependence of A_{CO_2} , indicating that current density significantly affects adsorption—desorption of ${\rm CO_2}$ molecules on the anode surface. This suggests that both temperature and electrochemical reactions could influence these adsorption—desorption of ${\rm CO_2}$. In both proposed LHHW models, the frequency of adsorption at a current density near 500 A/m² slightly increases and then decreases at a current density of 1000 A/m². However, these changes are more significant in dual-site models, as observed in Table 4 and Fig. 5. Furthermore, in all four LHHW models, the direction of equilibrium or reverse reaction direction may not significantly influence the frequency

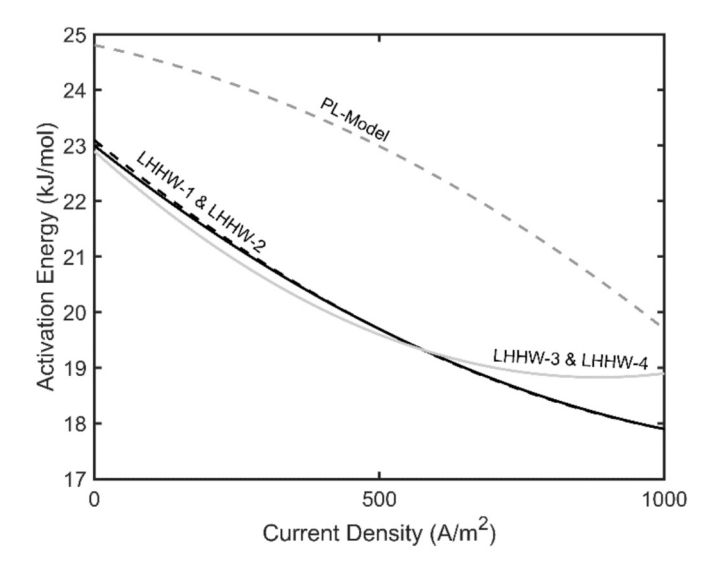


Fig. 3. The trend analysis of the current density effects on the activation energy for the DRM-SOFC process. The grey dashed line corresponds to the PL model, the black solid and dashed line represent single-site models (LHHW-1, LHHW-2) respectively, and the grey solid line corresponds to the dual-site models (LHHW-3, LHHW-4).

of adsorption. Similar trends were observed in SRM-DRM studies [26,27] related to the A_{H_2O} . However, it is important to note that no references support this observation in DRM-SOFC, highlighting the need for future experimental works using various models to investigate further and confirm these findings.

3.5. Adsorption equilibrium constant (K_{CO_2})

Adsorption activates reactants by binding them to the catalyst surface, while products leaves the surface by desorption. K_{CO_2} is the Langmuir adsorption constant for CO_2 , where a higher K_{CO_2} indicates stronger adsorption under specific conditions, influencing reaction rate and selectivity, and is the key for designing efficient anodes [19,44].

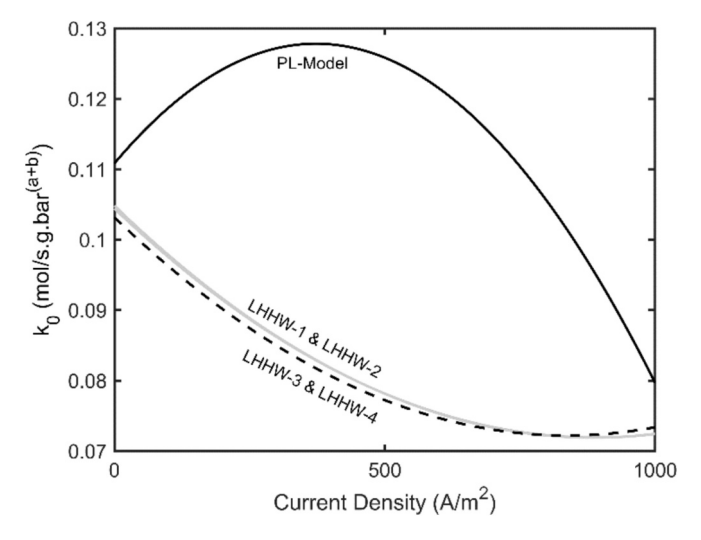


Fig. 4. The trend analysis of the current density effects on the pre-exponential factor of the rate constant for the DRM-SOFC process. The black solid line corresponds to the PL model, the grey solid line represents the single-site models, and the black dashed line corresponds to the dual-site models.

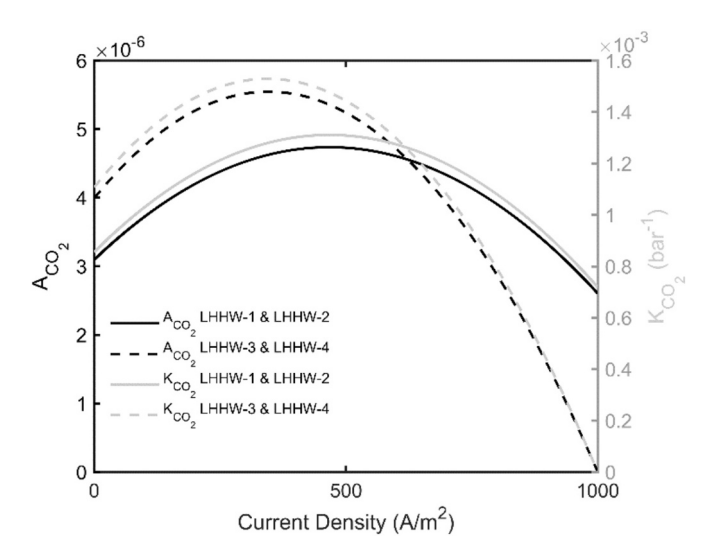


Fig. 5. The trend analysis of current density effects on the adsorption constant ($A_{\rm CO_2}$) and adsorption equilibrium constant ($K_{\rm CO_2}$) for the DRM-SOFC process in each proposed model. In the graph, the black solid line represents $A_{\rm CO_2}$ calculated by single-site models, the black dashed line corresponds to $A_{\rm CO_2}$ calculated by dual-site models, the grey solid line represents $K_{\rm CO_2}$ calculated by single-site models, and the grey dashed line corresponds to $K_{\rm CO_2}$ calculated by dual-site models.

 ${\rm CH_4}$ is known to be more competitive than ${\rm CO_2}$ for active metal sites on the catalyst surface [7]. Temperature enhances the adsorption and dissociation of reactants, reducing carbon deposition and suppressing catalyst deactivation [13,15,40]. In this study, the adsorption isotherm for ${\rm CH_4}$ is assumed not to be influenced by current density, given that ${\rm CH_4}$ mostly adsorbs on the catalyst surface. However, the impact of current density on $K_{{\rm CO_2}}$ is depicted in Fig. 5. The trend of $K_{{\rm CO_2}}$ changes with current density shows that, unlike temperature, current density exhibits non-uniform trends. The values of the adsorption constant reach their maximum near a current density of 500 ${\rm A/m^2}$ and decrease as further current is drawn from the fuel cell. According to van 't Hoff Eq. (4), the adsorption equilibrium constant depends on its pre-exponential factor, reflecting the frequency of adsorption—desorption events on the catalyst surface. Dual-site models, which consider more active sites, are expected to show more significant changes in $K_{{\rm CO_2}}$ with current density

compared to single-site models. This study confirms the expectation. However, a recent study [4] using the simplified LH model found that increasing current density from OCV to $1000~\text{A/m}^2$ significantly raised the CO_2 adsorption equilibrium constant, highlighting a positive current density effect. This contrasts with the current study's non-uniform K_{CO_2} trends, suggesting that high current density might exceed limits where CO_2 dissociative adsorption assumptions are valid, indicating a need for further research.

SRM and DRM in SOFCs are different processes but share similarities, as both reform methane with oxidants (CO₂ and H2O). Fan et al. reported a decreasing adsorption constant for steam in SRM-SOFCs [26], while Zhou et al.[27] observed a significant drop in the adsorption coefficient at 600 A/m², with a slight increase at 1000 A/m². These contradictory results for DRM and SRM suggest that more tests at smaller intervals are needed to validate these phenomena. Understanding the variations in chemical and electrochemical reactions in SOFC anodes is still evolving. These findings represent progress, but further research is necessary to grasp the full impact of current density on adsorption isotherms.

Beyond adsorption effects, electrochemical reactions significantly influence DRM–SOFC kinetics through their interaction with charge transfer and oxygen ion transport. The applied current density governs the flux of $\mathrm{O^{2-}}$ ions from the electrolyte to the anode surface, altering the local oxygen chemical potential and reaction energetics. These oxygen ions participate in the oxidation of $\mathrm{H_{2}}$ and CO near the TPB, facilitating electron transfer and shifting the equilibrium of surface reactions. As a result, variations in current density modify apparent activation energies and reaction rates, reflecting the strong coupling between electrochemical processes and catalytic reforming.

3.6. Change of CO_2 adsorption enthalpy $(\Delta H_{CO_2}^0)$ and entropy $(\Delta S_{CO_2}^0)$

The influence of current density on the CO_2 adsorption enthalpy and entropy in all four LHHW models is illustrated in Fig. 6. Changes in the $\Delta H^0_{CO_2}$ and entropy $\Delta S^0_{CO_2}$ indicates a robust role of electrochemical reaction during the adsorption process[38,47]. A negative $\Delta H^0_{CO_2}$ indicates exothermic CO_2 adsorption, while $\Delta S^0_{CO_2}$'s sign and magnitude reveal whether the adsorption is associative or dissociative. Negative $\Delta S^0_{CO_2}$ suggests an associative mechanism [11,19]. $\Delta H^0_{CO_2}$ is similar across all

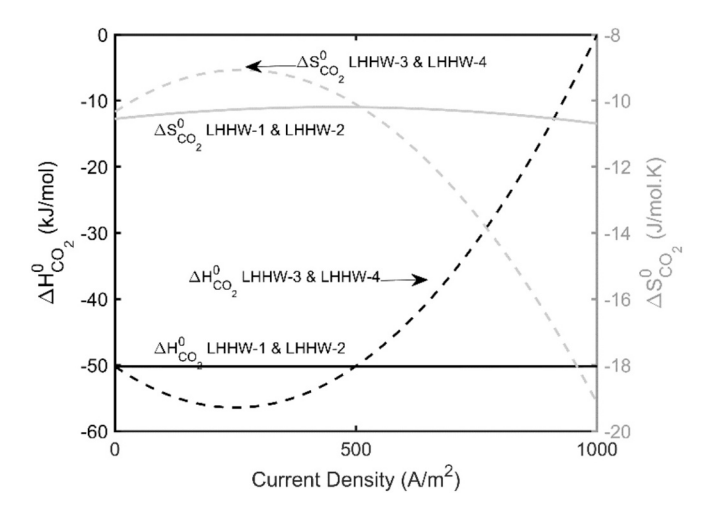


Fig. 6. The effect of the current density effects on the adsorption enthalpy $(\Delta H^0_{\text{CO}_2})$ and entropy $(\Delta S^0_{\text{CO}_2})$ for the DRM-SOFC process. The black solid line represents $\Delta H^0_{\text{CO}_2}$ in the single-site models, the black dashed line corresponds to $\Delta H^0_{\text{CO}_2}$ in the dual-site models, the grey solid line represents $\Delta S^0_{\text{CO}_2}$ in the single-site models, and the grey dashed line corresponds to $\Delta S^0_{\text{CO}_2}$ in the dual-site models.

models at open-circuit conditions, decreasing slightly and increasing with current density in dual-site models while remaining stable in single-site models. $\Delta S_{\text{CO}_2}^0$ increases by 10 J/(mol·K) in dual-site models with current density, indicating a stronger CO2 attachment. This shows that the driving force minimises CO2 adsorption enthalpy and entropy across all LHHW models (LHHW-1 to LHHW-4). Since dual-site models (LHHW-3 to LHHW-4) assume more active sites, changes in adsorption enthalpy and entropy with current density are more significant than in single-site models. Similar trends for H2O have been reported by Fan et al. [26] and Zhou et al. [27], but further research with diverse models and current densities in DRM-SOFCs is needed. A summary of the derived kinetic parameters in comparison with previously reported values for Ni-based catalysts is presented in Table 5, demonstrating that the parameters obtained in this study fall within the literature-reported ranges and thereby validate the accuracy of the proposed kinetic models.

3.7. Gibbs free energy change $\Delta G_{CO_2}^0$

For significant adsorption, Gibbs free energy change of adsorption, ΔG^0 , must be negative [19]. As a general guideline, significant adsorption requires a negative change in Gibbs free energy, and a decrease in the negative value of ΔG^0 with increasing current density from the cell suggests that the adsorption process becomes more favorable at higher current densities and vice versa[48]. This is often attributed to the increased mobility of adsorbate ions through the triple phase boundary (TPB) and the higher affinity of the CO_2 for the adsorbent at elevated current densities[4]. A negative ΔG^0 indicates a spontaneous process, whereas a positive ΔG^0 suggests a non-spontaneous process[38,42].

Fig. 7 shows that the values of $\Delta G_{\text{CO}_2}^0$ are similar across all models under open-circuit conditions. The single site models show constant $\Delta G_{\mathrm{CO}_2}^0$ across all current densities investigated in this study. However, in dual-site models, there is a significant decrease in $\Delta G_{\text{CO}_2}^0$ with a small current density, indicating an increase in the possibility of spontaneous CO_2 adsorption. Conversely, with a higher current density, the $\Delta G_{CO_2}^0$ increases, suggesting a non-spontaneous CO2 adsorption. This implies that CO₂ adsorption is a non-spontaneous process in higher current densities and has an optimum current density level when a dual-site assumption is used. The reason for such changes lies in the fact that the Gibbs free energy of the adsorption equation is a function of adsorption enthalpy and entropy, as shown in Eq. (6). Since the sensitivity of adsorption enthalpy and entropy to changes of current density in dual site models are more significant than in single-site models, this effect on the Gibbs free energy changes similarly. These findings represent the first discussion of Gibbs free energy of CO2 adsorption in DRM-SOFC. Further investigation is needed to understand the reasons behind these observations fully.

3.8. DRM reaction rate (r_{DRM})

As detailed in our previous study [4], Fig. 8 compares DRM reaction rates at 1000 A/m^2 and 1073 K, calculated using kinetic models, with experimental data. Similar earlier study [4], the current results confirm that higher methane partial pressure enhances the DRM reaction rate. This suggests that the competition between CH_4 and CO_2 for adsorption sites on the catalyst, reduces the impact of CO_2 partial pressure. The

Table 5Comparison of some kinetic parameters derived in this study with values previously reported for dry reforming of methane over Ni-based catalysts.

| Parameter | This Study | Reported Range (Literature) | References |
|---|------------|--------------------------------|---------------|
| Activation Energy (Ea, kJ mol ⁻¹) | 17.9–24.8 | 18–27 | [11–13,15,17] |
| CO ₂ Reaction Order (b) | 0.29-0.32 | 0.25-0.40 | [25–27] |

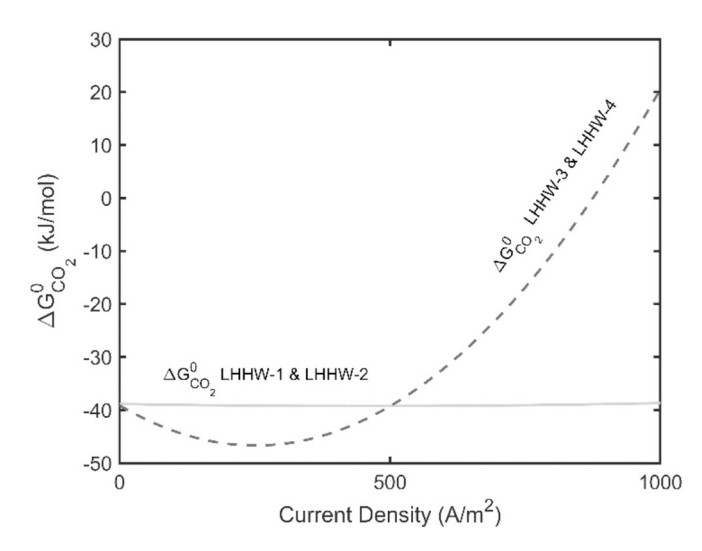


Fig. 7. The trend analysis of the current density effects on the Gibbs free energy change of CO_2 adsorption ($\Delta G^0_{CO_2}$) for the DRM-SOFC process. The grey solid line represents $\Delta G^0_{CO_2}$ in the single-site models, and the black dashed line corresponds to $\Delta G^0_{CO_2}$ in the dual-site models.

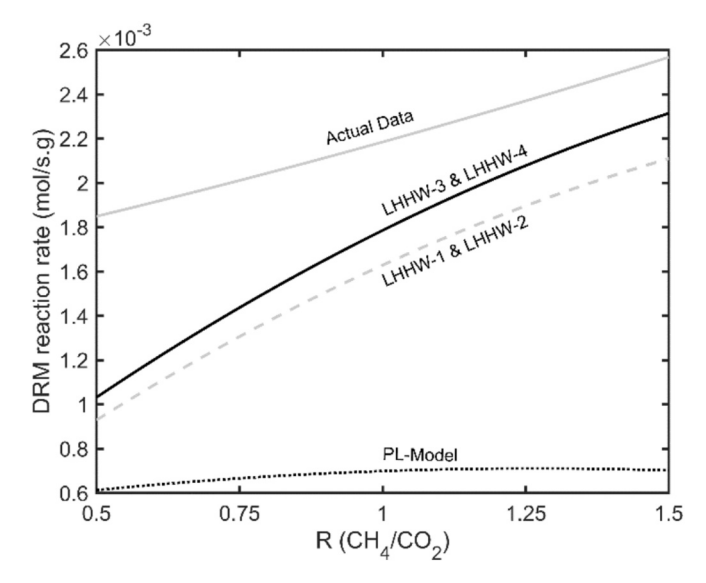


Fig. 8. DRM reaction rate calculation at 1073 K with a current density of 1000 A/m^2 to R ratios (CH₄ to CO₂ ratio) for DRM-SOFC process using proposed models. In the graph, the grey solid line represents actual reaction rate data, the black solid line corresponds to dual-site model estimation, the grey dashed line represents single-site model calculation, and the black dotted line corresponds to PL model estimation.

greater adsorption equilibrium constant for CH₄ than CO₂ may also contribute to this effect. Dual-site models (LHHW-3 to LHHW-4) showed the highest accuracy but performed poorly at lower R ratios. Zhou et al. [27] reported similar SRM-SOFC trends. However, the PL model failed to estimate the DRM reaction rate accurately. Our trend analysis shows that single-site models also deviate when fitting estimated reaction rates to actual data. Similar to other parameters, the direction of equilibrium or reverse reaction direction term in the rate expression has minimal impact on DRM-SOFC reaction rate estimation accuracy. Various researchers have used LHHW models for kinetic parameter extraction in DRM with different catalysts [11,13,15,17,19]. However, insufficient comprehensive studies on DRM-SOFC make comparisons challenging.

3.9. Model fitting and error evaluation

After determining the reaction rate constants at different temperatures, the activation energy was obtained by fitting the linearised Arrhenius equation (derived from Equation (9). The main aim of this study is to compare the PL and LH kinetic models and evaluate how their underlying assumptions affect the results. One of the criteria used was the coefficient of determination (R^2) from Equation (8). Kinetic parameters were estimated using non-linear regression in MATLAB®, minimising the root-mean-square error (RMSE) between experimental and predicted values. The RMSE was calculated as:

$$RMSE = \sqrt{\frac{1}{n} \sum_{i=1}^{n} \left(\frac{y_{exp,i} - y_{pred,i}}{y_{exp,i}} \right)^2}$$
 (11)

Where $y_{exp,i}$ and $y_{pred,i}$ are the experimental and model-predicted values, respectively, and n is the number of data points. Tri Nguyen et al.[11] compared calculated and experimental CH₄ consumption rates in DRM, finding that dual-site models yielded a lower *RMSE* and better fit than single-site models. Many studies also support the adsorption and activation of CH₄ and CO₂ on two distinct sites [19]. Table 6 summarizes model performance metrics for R^2 , adjusted R^2 , and *RMSE*.

The analysis of the models revealed significant performance differences. The PL model had a lower R^2 of 0.778 and an adjusted R^2 of 0.769, indicating a poorer fit to the data than the LHHW models. The LHHW models showed much higher R^2 values, ranging from 0.983 to 0.984, reflecting a better fit. Among them, dual-site models achieved the highest R^2 and adjusted R^2 values of 0.984 and 0.983, respectively. LHHW models had a lower *RMSE* than the PL model, with LHHW-3 and LHHW-4 showing the smallest *RMSE* of 4.78E-04. This indicates that LHHW models fit the data more accurately and offer better predictive precision, especially with dual-site models, which showed lower deviation from experimental data under the studied conditions.

Although the dual-site LHHW models (LHHW-3 to LHHW-4) performed best, their predictive capability remains limited by mechanistic simplifications. They primarily describe adsorption—desorption and surface reactions while neglecting carbon deposition, surface heterogeneity, and electrochemical effects. Carbon formation via methane cracking or the Boudouard reaction, and its partial gasification under electrochemical oxidation, can dynamically alter active sites and affect apparent kinetics. Variations in Ni–GDC–YSZ microstructure and oxygen ion flux near the triple-phase boundary further contribute to non-uniform behavior, meaning the derived parameters represent effective rather than purely intrinsic values.

The obtained kinetic models and parameters are directly applicable to system-level analyses and can be implemented in Computational Fluid Dynamics (CFD) or process simulation tools to model internal reforming in practical SOFC stacks. Their intrinsic nature and geometry independence allow prediction of methane conversion, temperature gradients, and electrochemical performance under varying fuel compositions and current densities. Integrating this kinetic framework into stack or system-scale simulations will support optimization of reactor design, operating conditions, and thermal management for large-scale DRM–SOFC applications.

Table 6 Model performance metrics for R^2 , adjusted R^2 , and *RMSE*.

| Model | R^2 | R ² Adjusted | RMSE |
|--------|-------|-------------------------|----------|
| PL | 0.778 | 0.769 | 1.52E-03 |
| LHHW-1 | 0.983 | 0.982 | 6.18E-04 |
| LHHW-2 | 0.983 | 0.982 | 6.18E-04 |
| LHHW-3 | 0.984 | 0.983 | 4.78E-04 |
| LHHW-4 | 0.984 | 0.983 | 4.78E-04 |

4. Conclusions

We investigated DRM-SOFC kinetics by considering various kinetic models, such as PL, LHHW and their derivations in an electrolyte-supported SOFC with a NiO-GDC-YSZ anode from 973 K to 1173 K, and a current density range from 0 to 1000 A/m². The current densities of employed in this study were intentionally chosen to ensure measurements in the intrinsic kinetic regime, thereby avoiding artefacts from mass and heat transfer limitations or ohmic losses. Using a small-area button cell (0.95 cm², 1 cm diameter, 50 μm electrolyte) and a catalyst mass of 14.3 mg in line with ICTAC recommendations further minimised transport effects. Although these values are lower than the operating current densities of commercial DRM-SOFCs, the kinetic parameters obtained are independent of cell size and operating current. They can therefore be applied to larger-scale system models when combined with transport and thermal management considerations, making them directly relevant to practical SOFC operation.

In terms of kinetic models, the PL model shows a notable increase in ${\rm CO_2}$ reaction order with a small current density, followed by a decrease at higher current density levels. All LHHW models exhibit similar reaction order values up to $500~{\rm A/m^2}$, but the single-site models diverge at higher current densities, with dual-site models displaying a decreasing trend. The inverse reactions or df minimally affect LHHW estimations of reaction order, and current density has an insignificant impact on ${\rm CO_2}$ reaction order within the investigated current density and temperature range.

Moreover, all four LHHW models (LHHW-1 to LHHW-4) has a lower activation energy than the PL model with the same current densities, probably due to its incorporation of surface reaction mechanisms. Differences in proposed mechanisms between single-site and dual-site LHHW models result in different activation energies, particularly at higher current densities. Furthermore, the reverse reaction minimally affects the activation energies. Depending on the reaction orders of the reactants, this study also reveals that the current density influences the pre-exponential factor (k_0). The PL model shows a peak in k_0 at a current density of 500 A/m² corresponding to higher CO₂ reaction orders, followed by a decrease with a higher current density. Despite non-uniform trends across the investigated current density range, we have also found that both PL and all LHHW models exhibit similar values at higher current densities.

The current density-dependent behavior of $A_{\rm CO_2}$ indicates the significant influence of electrochemical reaction on ${\rm CO_2}$ adsorption–desorption over the anode surface. Both LHHW models exhibit fluctuations in adsorption frequency, particularly in the dual-site models, showing peaks near 500 A/m² and declines at 1000 A/m². Moreover, the inverse reaction shows minimal impact on the adsorption frequency across all LHHW models. The analysis of this study reveals the non-uniform trends in $K_{\rm CO_2}$ changes with current density. The adsorption equilibrium constant peaks near 500 A/m² and decreases with a higher current density. Dual-site assumptions are expected to magnify these changes because more active sites are assumed, yet findings contradict expectations and previous studies. Conducting additional tests with smaller intervals may clarify these discrepancies and validate the observed trends in the dependency of the adsorption equilibrium constant on the current density.

Also, we found that the values of $\Delta H^0_{\mathrm{CO}_2}$ remain consistent across all proposed models under open-circuit conditions while fluctuating with current density, particularly in dual-site models. The single-site models exhibit stable trends, and the dual-site models show a notable increase in $\Delta S^0_{\mathrm{CO}_2}$ with higher current densities. $\Delta G^0_{\mathrm{CO}_2}$ remain consistent in all models under open-circuit conditions. The single-site models maintain a constant $\Delta G^0_{\mathrm{CO}_2}$ across the investigated current density range, whereas the dual-site models show a notable increase in $\Delta G^0_{\mathrm{CO}_2}$ at higher current densities, indicating an increased spontaneous CO_2 adsorption. Similar to other kinetic parameters, the direction of equilibrium or reverse

reaction direction (driving force df) as the numerator in reaction rate expression has negligible effects on the CO_2 adsorption enthalpy and entropy and Gibbs free energy of CO_2 adsorption in all LHHW models. However, further exploration of different models with a broader range of current densities is recommended to understand these observations in DRM-SOFC better.

Additionally, comparing the simulated and experimental reaction rates at a current density of 1000 A/m² and T = 1073 K reveals that the dual-site models offer the highest accuracy with various methane-tocarbon dioxide ratios. While dual-site models show improved accuracy at higher methane-to-carbon dioxide ratios, they exhibit relatively low accuracy at lower methane-to-carbon dioxide ratios. Conversely, the PL model fails to estimate DRM reaction rates accurately in this study. The LHHW models, especially the dual-site variants, significantly outperform the PL model. All four LHHW models (LHHW-1 to LHHW-4) achieved much higher R² values (0.983 to 0.984) and lower RMSE (4.78E-04) than the PL model, 0.778 and higher RMSE. This indicates that the LHHW models, with their dual-site versions, provide a more accurate fit and better predictive precision for kinetic parameters in DRM-SOFC. The trend analysis suggests that the single-site models deviate when fitting estimated reaction rates to the experimental data. The inverse reaction term in the LHHW model rate expressions in Table 3 has a negligible effect on the estimation accuracy of the reaction rate in the DRM-SOFC. Our findings provide essential parameters for future simulation studies.

This study uniquely quantifies the adsorption enthalpy, entropy, and Gibbs free energy of CO_2 adsorption in a DRM–SOFC system, introducing a thermodynamic perspective that distinguishes it from previous kinetic studies. Although the dual-site LHHW models ((LHHW-3 to LHHW-4) showed the best agreement with experiments, their accuracy remains limited due to unaccounted carbon deposition effects at the triple-phase boundary, indicating a need for further refinement of kinetic/electrochemical models. The derived parameters are directly applicable to CFD and system-level SOFC simulations, providing validated inputs for optimizing reforming performance, temperature management, and fuel utilization in practical DRM–SOFC systems.

5. Future studies

S. Moarrefi et al.

Future studies will expand the current intrinsic kinetic framework to address additional complexities relevant to practical DRM-SOFC operation. These include side reactions (e.g. methane cracking), hydrogen consumption via electrochemical oxidation, catalyst deactivation mechanisms (e.g., carbon deposition, Ni coarsening), and long-term durability under realistic load cycles. Such factors will be incorporated into coupled kinetic–transport models and validated through extended experimental campaigns. This approach will enable a more comprehensive prediction of DRM-SOFC performance and bridge the gap between intrinsic kinetics and long-term system behaviour. Future work will compare kinetic behaviour under fixed-bed and plug-flow assumptions, assess the impact of including the forward WGS reaction at lower temperatures or under steam reforming conditions, and explicitly model an electrochemically assisted $\mathrm{CH_4}$ and $\mathrm{CO_2}$ activation pathway to clarify how electrochemical effects influence intrinsic DRM kinetics.

CRediT authorship contribution statement

Saeed Moarrefi: Writing – review & editing, Writing – original draft, Validation, Software, Methodology, Investigation, Formal analysis, Data curation. Mohan Jacob: Supervision. Shou-Han Zhou: Writing – review & editing, Supervision, Software. Stephen Skinner: Supervision. Lichao Jia: Writing – review & editing, Supervision. Weiwei Cai: Writing – review & editing, Supervision. Liyuan Fan: Writing – review & editing, Visualization, Validation, Supervision, Software, Resources, Project administration, Methodology, Investigation, Funding acquisition, Formal analysis, Conceptualization.

Declaration of competing interest

The authors declare that they have no known competing financial interests or personal relationships that could have appeared to influence the work reported in this paper.

Acknowledgement

The authors thank National Key R&D Program of China (2024YFF0506300) for the financial support, James Cook University, Australia, for providing educational resources and the International Collaboration for Hydrogen Research Program, Australia, for supporting international research collaborations.

Appendix A. Supplementary data

Supplementary data to this article can be found online at https://doi.org/10.1016/j.fuel.2025.137517.

Data availability

Data will be made available on request.

References

- U. Nations, The Glasgow Climate Pact Key Outcomes from COP26, 2021. https:// unfccc.int/process-and-meetings/the-paris-agreement/the-glasgow-climate-pactkey-outcomes-from-cop26. (Accessed 13 December 2021).
- [2] NASA, Methane, latest measurment in December 2023, 2023. https://climate. nasa.gov/vital-signs/methane/?intent=121. 2024).
- [3] Achakulwisut P, Erickson P, Guivarch C, Schaeffer R, Brutschin E, Pye S. Global fossil fuel reduction pathways under different climate mitigation strategies and ambitions. Nat Commun 2023;14(1):5425. https://doi.org/10.1038/s41467-023 41105-z.
- [4] S. Moarrefi, M. Jacob, C.e. Li, W. Cai, L. Fan, Internal dry reforming of methane in solid oxide fuel cells, Chemical Engineering Journal 489 (2024) 151281. https://doi.org/https://doi.org/10.1016/j.cej.2024.151281.
- [5] L. Fan, C.e. Li, L. van Biert, S.-H. Zhou, A.N. Tabish, A. Mokhov, P.V. Aravind, W. Cai, Advances on methane reforming in solid oxide fuel cells, Renewable and Sustainable Energy Reviews 166 (2022) 112646. https://doi.org/https://doi.org/10.1016/i.rser.2022.112646.
- [6] Abouemara K, Shahbaz M, McKay G, Al-Ansari T. The review of power generation from integrated biomass gasification and solid oxide fuel cells: current status and future directions. Fuel 2024;360:130511. 10.1016/j.fuel.2023.130511.
- [7] L. Fan, C.e. Li, P.V. Aravind, W. Cai, M. Han, N. Brandon, Methane reforming in solid oxide fuel cells: Challenges and strategies, Journal of power sources 538 (2022). https://doi.org/10.1016/j.jpowsour.2022.231573.
- [8] H.H. Faheem, B. Britt, M. Rocha, S.-H. Zhou, C.e. Li, W. Cai, L. Fan, Sensitivity analysis and process optimization for biomass processing in an integrated gasifiersolid oxide fuel cell system, Fuel 356 (2024) 129529. https://doi.org/https://doi. org/10.1016/j.fuel.2023.129529.
- [9] Najafi Maharluie H, Rahmani M. Mathematical modeling of solid oxide fuel cell performance with indirect internal reforming and thermal interaction analysis. Energy Conversion and Management 316 2024;118842. 10.1016/j.enconman.20 24.118842
- [10] Li H, Wei W, Zhang T, Liu F, Xu X, Li Z, et al. Degradation mechanisms and mitigation strategies of direct methane solid oxide fuel cells. Appl Energy 2024; 359:122609. 10.1016/j.apenergy.2023.122609.
- [11] Nguyen T, Luu CL, Phan HP, Nguyen PA, Van Nguyen TT. Methane dry reforming over nickel-based catalysts: insight into the support effect and reaction kinetics. React Kinet Mech Catal 2020;131(2):707–35. https://doi.org/10.1007/s11144-020-01876-8
- [12] L. Pino, C. Italiano, M. Laganà, A. Vita, V. Recupero, Kinetic study of the methane dry (CO2) reforming reaction over the Ce0.70La0.20Ni0.10O2–δ catalyst, Catalysis Science & Technology 10(8) (2020) 2652-2662. https://doi.org/ 10.1039/C9CY02192B.
- [13] Sandoval-Bohórquez VS, Morales-Valencia EM, Castillo-Araiza CO, Ballesteros-Rueda LM, Baldovino-Medrano VG. Kinetic Assessment of the Dry Reforming of Methane over a Ni–La2O3 Catalyst. ACS Catal 2021;11(18):11478–93. https://doi.org/10.1021/acscatal.1c02631.
- [14] Hou K, Hughes R. The kinetics of methane steam reforming over a Ni/ α -Al2O catalyst. Chem Eng J 2001;82(1):311–28. 10.1016/S1385-8947(00)00367-3.
- [15] Kathiraser Y, Oemar U, Saw ET, Li Z, Kawi S. Kinetic and mechanistic aspects for CO2 reforming of methane over Ni based catalysts. Chem Eng J 2015;278:62–78. 10.1016/j.cej.2014.11.143.
- [16] Yang KZ, Twaiq F. Modelling of the dry reforming of methane in different reactors: a comparative study. React Kinet Mech Catal 2017;122(2):853–68. https://doi. org/10.1007/s11144-017-1277-9.

- [17] Mark MF, Maier WF, Mark F. Reaction kinetics of the CO2 reforming of methane. Chem Eng Technol 1997;20(6):361–70. 10.1002/ceat.270200602.
- [18] Abdullah B, Abd Ghani NA, Vo D-V-N. Recent advances in dry reforming of methane over Ni-based catalysts. Journal of Cleaner Production 162 2017:170–85. 10.1016/j.jclepro.2017.05.176.
- [19] M.A. Vannice, Kinetic Data Analysis and Evaluation of Model Parameters for Uniform (Ideal) Surfaces, in: M.A. Vannice (Ed.), Kinetics of Catalytic Reactions, Springer US, Boston, MA, 2005, pp. 106-140. https://doi.org/10.1007/978-0-387-25972-7 6.
- [20] Moarrefi S, Jacob M, Shah N, Skinner S, Cai W, Fan L. Comparison of steam and dry reforming adsorption kinetics in solid oxide fuel cells. Fuel 2025;388:134413. 10 1016/j. fuel 2025 134413
- [21] Li Y, Wang Y, Wu J, Gao S, Zhu B, Wang J, et al. Catalytic performance of NixCoy catalysts supported on honeycomb-lantern-like CeO2 for dry reforming of methane: Synergistic effect and kinetic study. Chem Eng Sci 2024;291:119906. 10 1016/j.ces.2024.119906.
- [22] E.A. Nakajima, L.G. Oliveira, L.J. Gasparrini, G.E.d.Q. Souza, A.A. Ignacio, H.J. Alves, C.E. Borba, Kinetics of dry reforming of methane catalyzed by Ni/Si-MCM-41, International Journal of Hydrogen Energy 48(83) (2023) 32331-32341. https://doi.org/https://doi.org/10.1016/j.ijhydene.2023.05.010.
- [23] Wittich K, Krämer M, Bottke N, Schunk SA. Catalytic Dry Reforming of Methane: Insights from Model Systems. ChemCatChem 2020;12(8):2130–47. 10.1002/cctc. 201902142
- [24] L. Fan, L. van Biert, A. Thallam Thattai, A.H.M. Verkooijen, P.V. Aravind, Study of Methane Steam Reforming kinetics in operating Solid Oxide Fuel Cells: Influence of current density, International Journal of Hydrogen Energy 40(15) (2015) 5150-5159. https://doi.org/https://doi.org/10.1016/j.ijhydene.2015.02.096.
- [25] Thallam Thattai A, van Biert L, Aravind PV. On direct internal methane steam reforming kinetics in operating solid oxide fuel cells with nickel-ceria anodes. Journal of Power Sources 370 2017:71–86. 10.1016/j.jpowsour.2017.09.082.
- [26] Fan L, Mokhov A, Saadabadi SA, Brandon N, Aravind PV. Methane steam reforming reaction in solid oxide fuel cells: Influence of electrochemical reaction and anode thickness. J Power Sources 2021;507:230276. 10.1016/j.jpowsour.2021.230276.
- [27] Zhou S-H, Omanga E, Tabish AN, Cai W, Fan L. Effect of electrochemical reaction on steam adsorption during methane reforming on a Ni-GDC anode. Fuel 2023;332: 125973. 10.1016/j.fuel.2022.125973.
- [28] Wójcik M, Szabłowski Ł, Dybiński O. Comparison of mathematical models of steam methane reforming process for the needs of fuel cells. Int J Hydrogen Energy 2024; 52:965–82. 10.1016/j.ijhydene.2023.08.293.
- [29] S.A. Saadabadi, A. Thallam Thattai, L. Fan, R.E.F. Lindeboom, H. Spanjers, P.V. Aravind, Solid Oxide Fuel Cells fuelled with biogas: Potential and constraints, Renewable energy 134 (2019) 194-214. https://doi.org/10.1016/j.renene.2018.11.028.
- [30] Mogensen D, Grunwaldt JD, Hendriksen PV, Dam-Johansen K, Nielsen JU. Internal steam reforming in solid oxide fuel cells: Status and opportunities of kinetic studies and their impact on modelling. J Power Sources 2011;196(1):25–38. 10.1016/j. ipowsour.2010.06.091.
- [31] Vyazovkin S, Burnham AK, Criado JM, Pérez-Maqueda LA, Popescu C, Sbirrazzuoli N. ICTAC Kinetics Committee recommendations for performing kinetic computations on thermal analysis data. Thermochim Acta 2011;520(1):1–19. 10 1016/j.ica.2011.03.034.
- [32] Karabanova A, Berdiyeva P, van der Pal M, Johnsen RE, Deledda S, Blanchard D. Intrinsic kinetics in local modelling of thermochemical heat storage systems. Appl Therm Eng 2021;192:116880. 10.1016/j.applthermaleng.2021.116880.

- [33] Priest CM, Gomez JY, Kane NJ, Hartvigsen JL, Wang L, Ding D, et al. Challenges in practical button cell testing for hydrogen production from high temperature electrolysis of water. Front Energy Res 2023;11–2023. https://doi.org/10.3389/ fenrs 2023.1278203
- [34] Machaj K, Kupecki J, Niemczyk A, Malecha Z, Brouwer J, Porwisiak D. Numerical analysis of the relation between the porosity of the fuel electrode support and functional layer, and performance of solid oxide fuel cells using computational fluid dynamics. Int J Hydrogen Energy 2024;52:936–51. 10.1016/j.ijhydene.20 23.06.166.
- [35] Guerra C, Lanzini A, Leone P, Santarelli M, Brandon NP. Optimization of dry reforming of methane over Ni/YSZ anodes for solid oxide fuel cells. J Power Sources 2014;245:154–63. 10.1016/j.jpowsour.2013.06.088.
- [36] Fan L, Qu Z, Pourquie MJBM, Verkooijen AHM, Aravind PV. Computational Studies for the Evaluation of Fuel Flexibility in Solid Oxide Fuel Cells: A Case with Biosyngas. Fuel Cells (Weinheim an der Bergstrasse, Germany) 2013;13(3):410–27. https://doi.org/10.1002/fuce.201200138.
- [37] Fan L, Dimitriou E, Pourquie MJBM, Liu M, Verkooijen AHM, Aravind PV. Prediction of the performance of a solid oxide fuel cell fuelled with biosyngas: Influence of different steam-reforming reaction kinetic parameters. Int J Hydrogen Energy 2013;38(1):510–24. 10.1016/j.ijhydene.2012.09.061.
- [38] W. Winkler, P. Nehter, Thermodynamics of Fuel Cells, in: R. Bove, S. Ubertini (Eds.), Modeling Solid Oxide Fuel Cells: Methods, Procedures and Techniques, Springer Netherlands, Dordrecht, 2008, pp. 13-50. https://doi.org/10.1007/978-1-4020-6995-6 2.
- [39] van Biert L, Godjevac M, Visser K, Aravind PV. Dynamic modelling of a direct internal reforming solid oxide fuel cell stack based on single cell experiments. Appl Energy 2019;250:976–90. 10.1016/j.apenergy.2019.05.053.
- [40] Faheem HH, Abbas SZ, Tabish AN, Fan L, Maqbool F. A review on mathematical modelling of Direct Internal Reforming- Solid Oxide Fuel Cells. J Power Sources 2022;520:230857. 10.1016/j.jpowsour.2021.230857.
- [41] O. Levenspiel, Chemical reaction engineering, John wiley & sons1998.
- [42] Wang W-Y, Wang G-C. The first-principles-based microkinetic simulation of the dry reforming of methane over Ru(0001). Cat Sci Technol 2021;11(4):1395–406. https://doi.org/10.1039/D0CY01942A.
- [43] Peleg M, Normand MD, Corradini MG. The Arrhenius Equation Revisited. Crit Rev Food Sci Nutr 2012;52(9):830–51. https://doi.org/10.1080/ 10408398.2012.667460.
- [44] Minette F, Lugo-Pimentel M, Modroukas D, Davis AW, Gill R, Castaldi MJ, et al. Intrinsic kinetics of steam methane reforming on a thin, nanostructured and adherent Ni coating. Appl Catal B 2018;238:184–97. 10.1016/j.apcatb.2018.07.01
- [45] Christov SG. Collision Theory and Statistical Theory of Chemical Reactions. Berlin Heidelberg: Springer; 2012.
- [46] Yusuf M, Beg M, Ubaidullah M, Shaikh SF, Keong LK, Hellgardt K, et al. Kinetic studies for DRM over high-performance Ni–W/Al2O3–MgO catalyst. Int J Hydrogen Energy 2022;47(100):42150–9. 10.1016/j.ijhydene.2021.08.021.
- [47] Lima EC, Gomes AA, Tran HN. Comparison of the nonlinear and linear forms of the van't Hoff equation for calculation of adsorption thermodynamic parameters (ΔS° and ΔH°). J Mol Liq 2020;311:113315. 10.1016/j.molliq.2020.113315.
- [48] Du X, Cheng Y, Liu Z, Yin H, Wu T, Huo L, et al. CO2 and CH4 adsorption on different rank coals: A thermodynamics study of surface potential. Gibbs free energy change and entropy loss, Fuel 2021;283:118886. 10.1016/j.fuel.2020.11 8886